

Published in final edited form as:

*Plant J.* 2013 November ; 76(4): 627–633. doi:10.1111/tpj.12322.

## Contrasting calcium localization and speciation in leaves of *Medicago truncatula* mutant COD5 analyzed via synchrotron X-ray techniques

Tracy Punshon<sup>1,\*</sup>, Ryan Tappero<sup>2</sup>, Felipe K. Ricachenevsky<sup>3</sup>, Kendal Hirschi<sup>4,5</sup>, and Paul A. Nakata<sup>5</sup>

Ryan Tappero: rtappero@bnl.gov; Felipe K. Ricachenevsky: felipecruzalta@yahoo.com.br; Kendal Hirschi: kendalh@bcm.edu; Paul A. Nakata: pnakata@bcm.edu

<sup>1</sup>Life Sciences Center, Dartmouth College, Hanover, NH, 03755, USA. Tel: (603) 646 1037

<sup>2</sup>Photon Sciences Directorate, National Synchrotron Light Source, Brookhaven National Laboratory, Upton, NY 11973

<sup>3</sup>Universidade Federal do Rio Grande do Sul, Centro de Biotecnologia, Porto Alegre, Brazil

<sup>4</sup>Vegetable and Fruit Improvement Center, Texas A&M University, College Station, Texas 77845

<sup>5</sup>United States Department of Agriculture/Agriculture Research Service, Children's Nutrition Research Center, Department of Pediatrics, Baylor College of Medicine, Houston, Texas 77030

### SUMMARY

Oxalate-producing plants accumulate calcium oxalate crystals ( $\text{CaOx}_{(c)}$ ) in the range of 3–80% (w/w) of their dry weight, reducing calcium (Ca) bioavailability. The *calcium oxalate deficient 5* (*cod5*) mutant of *Medicago truncatula* has been previously shown to contain similar Ca, but lower oxalate and  $\text{CaOx}_{(c)}$  concentrations than wild type (WT) plants. We imaged the Ca distribution in WT and *cod5* leaflets via synchrotron X-ray fluorescence mapping (SXRF). We observed a contrast in the Ca distribution between *cod5* and WT leaflets, manifested as an abundance of Ca in the interveinal areas and a lack of Ca along the secondary veins in *cod5*, the opposite of WT. X-ray microdiffraction ( $\mu\text{XRD}$ ) of *M. truncatula* leaves confirmed crystalline  $\text{CaOx}_{(c)}$  (whewellite;  $\text{CaC}_2\text{O}_4 \cdot \text{H}_2\text{O}$ ) was present in WT only, in cells sheathing the secondary veins. Together with  $\mu\text{XRD}$ , microbeam Ca K-edge X-ray absorption near-edge structure spectroscopy ( $\mu\text{XANES}$ ) indicated that among the forms of CaOx – namely crystalline or amorphous – only amorphous CaOx was present in *cod5*. These results demonstrate that deletion of *COD5* changes both Ca localization and the form of CaOx within leaflets.

### INTRODUCTION

Crystalline calcium oxalate ( $\text{CaOx}_{(c)}$ ) occurs naturally in more than 215 plant families (McNair, 1932), including a number of agriculturally important crop species. As much as 90% (w/w) of the total plant calcium (Ca) can be bound as the oxalate salt (Nakata and McConn, 2003). While crystal formation is common, it suppresses Ca bioavailability (Franceschi and Nakata, 2005), this preventing crystal formation is a valid approach for enhancing Ca bioavailability in crop plants.

For correspondence (tracy.punshon@dartmouth.edu).

The authors declare no conflict of interest.

Little is known about how  $\text{CaOx}_{(C)}$  occurs in plants and what function crystals play in growth and development (reviewed by (Webb, 1999; Bauer et al., 2011; Nakata, 2012). The diversity of crystal sizes, as well as their prevalence and spatial distribution, have led to numerous hypotheses about their function in ion balance, plant defense, tissue rigidity, detoxification, light gathering and reflection (Franceschi and Horner, 1980) (Franceschi and Nakata, 2005). However, not all plants make  $\text{CaOx}_{(C)}$  and there are limited studies addressing how Ca partitioning and sequestration differs among plant types.

A Ca oxalate defective mutant of the model forage legume *Medicago truncatula*, *cod5* was identified previously in a genetic screen by its inability to accumulate prismatic crystals of  $\text{CaOx}_{(C)}$  in its leaflets (Nakata and McConn, 2000). Growth studies and total mineral composition measurements indicate no detectable difference between *cod5* and wild type (WT) with the exception of oxalate levels (Nakata and McConn, 2000; Nakata, 2003; Nakata and McConn, 2003, 2006). Feeding studies showed that mice fed diets containing extrinsically and intrinsically  $^{45}\text{Ca}$ -labeled WT and *cod5* *M. truncatula* absorbed significantly more Ca (22.8%) from *cod5* plants compared to WT (Morris et al., 2007).

The objective of this study was to compare the distribution and speciation of Ca in *cod5* and WT leaflets. Investigations of biogenic  $\text{CaOx}_{(C)}$  in plant tissues using X-ray powder diffraction were reported as early as 1980 (Schadel and Walter Jr, 1980; Horner and Zindler-Frank, 1982), and X-ray Absorption Near-Edge Structure (XANES) spectroscopy has been used to explore Ca speciation in the trichomes of Tobacco plants (Sarret et al., 2007). More recently, Yamauchi et al (2013) used SXRF in three dimensional microtomography mode to show that crystals of Ca oxalate were distributed along the lateral veins on the abaxial side of the procambium in the embryonic cotyledons of *Lotus miyakojimae*.

The novelty of this work lies in uncovering a Ca distribution phenotype in *cod5*. SXRF is particularly informative when it is used to image the changes in elemental distribution that result from genetic mutations (Kim et al., 2006), and this has become a useful tool in gene characterization (Punshon et al., 2013).

## RESULTS

### Ca and oxalate levels

To check that Ca and oxalate concentration of WT and *cod5* plant tissues were consistent with previously published studies (Nakata and McConn, 2000; Nakata, 2003; Nakata and McConn, 2003; Franceschi and Nakata, 2005; Korth et al., 2006; Nakata and McConn, 2006; Nakata, 2012), WT and *cod5* mutant plants were grown hydroponically as previously reported (Nakata and McConn, 2006). Measurements of WT leaflets showed a total oxalate level of about  $17 \text{ mg g}^{-1}$  dry weight (DW) (Table 1). Oxalate levels in *cod5* were drastically lower at approximately  $2 \text{ mg g}^{-1}$  dry weight (Table 1). We also measured whether Ca levels corresponded with the reduction in total oxalate content and confirmed that no difference in Ca concentration was found between WT and the *cod5* mutant.

### Ca distribution in leaflets

To determine whether Ca distribution was changed in *cod5* relative to WT, SXRF elemental maps of Ca were collected from dried, whole *Medicago* leaflets from both WT and *cod5* at 4100 eV (Figure 1). Maps show a strong secondary vein-associated Ca distribution in WT, and an inverse, intervein-associated Ca distribution in *cod5*. Cryosectioned, thawed leaflets analyzed at 11 keV show the Ca localization of WT in cross-section (Figure 2), with Ca-enriched cells, which we hypothesize to be crystal idioblasts, located above and below the secondary veins. It is not clear from the resolution of these maps whether these cells were

part of the epidermal layer, or distinct from it. These maps were not used to compare Ca abundances between WT and *cod5* because of the effects of detector saturation and increased dead time on the fluorescence counts at 4100eV. Abundance comparisons were conducted on the same samples, re-imaged at 11 keV. Notably, edge-jump direct measurement of the number of Ca atoms showed that *cod5* had 25% higher Ca atoms in intervein tissue than WT.

In both WT and *cod5* leaflets, K abundances were relatively higher in the secondary veins than in intervein tissue (Supplemental Figure 1). Because the spectral peak for K  $K\beta$  is close to that of Ca  $K\alpha$ , we checked that K fluorescence was not an artifact in Ca counts by subtracting K  $K\beta$  fluorescence from the spectra prior to quantification of Ca in these tissues. Analysis of micronutrients Fe, Mn, Cu and Zn showed no quantitative or qualitative changes between WT and *cod5*, and are not shown.

## Diffraction

In order to confirm the presence of  $\text{CaOx}_{(c)}$  in WT *Medicago* leaflets without interference from other Ca-containing structures such as cell walls, we collected X-ray microdiffraction patterns from Ca-enriched cells of WT leaflets exposed in cross-section. While the diffraction volume was small and reflections were weak, the  $\mu\text{XRD}$  data from Ca-enriched cells in WT are consistent with a hydrated CaOx mineral whewellite ( $\text{CaC}_2\text{O}_4 \cdot \text{H}_2\text{O}$ ); d-spacings measured were 2.34, 2.28, 2.07, 1.93, 1.73, and the comparable d-spacings for the whewellite standard were 2.34, 2.25, 2.07, 1.92, and 1.73.

## Spectroscopy

To identify any differences in the Ca binding form between WT and *cod5*, we conducted  $\mu\text{XANES}$  analysis on both freeze-dried whole leaflets and of cryo-sectioned, thawed leaflets. Guided by the Ca elemental distribution (Figure 1) we focused the spectroscopy on the speciation of Ca in secondary vein and intervein tissue. Sample preparation – specifically cryo-sectioning fresh tissue – was conducted to expose the cells with CaOx crystals and other mesophyll cells of the vein and interveins respectively, removing the influence of Ca in cell walls, or epidermal cell layers on the final spectra.

We compared replicated, summed spectra to a range of candidate standard materials for linear recombination analysis. Figure 3a shows the  $\mu\text{XANES}$  spectra for the complete set of standard reference materials considered for the linear combination fitting of experimental spectra, and Figure 3b shows enlargement of the main peaks for Ca-pectate, CaOx, and Ca-citrate. XANES spectra for Ca-pectate, CaOx and Ca-citrate have important distinguishing features. The energy of the ‘white line’ peak (the absorption maxima) for Ca-pectate (4045.8 eV) is higher than both Ca-citrate and CaOx (4044.8 eV). Differences between Ca-citrate and CaOx are subtle; CaOx has a unique feature after the absorption edge at 4052.5 eV, whereas Ca-citrate has a beat on the first oscillation at 4074.7 eV.  $\mu\text{XANES}$  is a short-range probe, sensitive only to the local coordination environment (2 to 3 atomic shells) around the central absorbing atom, therefore compounds with a similar local structure, such as Ca complexes with low molecular weight organic acids, will have similar XANES spectra. For example, Ca-citrate (1:1 complex) consists of a Ca atom chelated by the citrate molecule with bonding via three oxygen atoms from two COOH groups and one hydroxyl group (i.e. tridentate). From the  $\mu\text{XANES}$  (local) perspective, it is a Ca atom with 8-fold oxygen coordination in the first shell (3 from citrate) and 3 C atoms at slightly different distances in the second shell. This local coordination environment would be similar for other Ca compounds where a tricarboxylate ligand is bound to Ca, such as Ca-aconitate. Therefore, other tri-carboxylate bound Ca species will be represented in the estimate of Ca-citrate and likewise for di-carboxylate bound Ca species in the estimate of CaOx. However, CaOx is

unique because both C atoms in the second shell occur at the same interatomic distance, symmetry that produces multiple scattering events. Ca-pectate also has a unique bonding environment where a Ca atom is lodged between two adjacent chains of the pectate polymer.

Calcium K-edge  $\mu$ XANES spectra from interveinal tissue of cryo-sectioned leaflets indicated that Ca speciation in WT and *cod5*, differs only with respect to the crystalline form of  $\text{CaOx}_{(c)}$ , which was altered in *cod5* (Figure 4). The relative edge-step of WT and *cod5* spectra (not visible from the edge-step normalized plot shown in Figure 4) showed that WT contain approximately 25% less Ca in interveinal tissue than *cod5*. For both interveinal tissue spectra, the lowest goodness-of-fit value (NSS) was obtained with the Ca-citrate standard reference. Adding Ca-pectate improved the NSS by greater than 20%, but not when CaOx was included; inclusion of a third component was not justified based on NSS. The Ca speciation in interveinal tissue was best modeled as a near equal mixture of Ca-citrate and Ca-pectate for both WT and *cod5* plants (Figure 5).

Ca K-edge  $\mu$ XANES spectra from secondary veins and intervein of freeze-dried, whole leaflets of WT gave a lowest goodness-of-fit value (NSS) with the CaOx standard (Figure 5; Table 2). Adding a second component improved the NSS by greater than 20% when Ca-pectate was included, but not when Ca-citrate or other Ca standards were included; inclusion of a third component was not justified based on NSS. Thus, the Ca speciation in WT veins is predominately CaOx (~90%) with some Ca-pectate (~10%).

Complimentary X-ray microdiffraction data confirmed WT veins contain X-ray crystalline CaOx (i.e.,  $\text{CaOx}_{(c)}$ ). For the remaining whole-leaflet spectra (i.e., WT intervein, *cod5* vein, and *cod5* intervein), a lowest goodness-of-fit value (NSS) was obtained with the Ca-citrate standard reference. Adding a second component improved the NSS by greater than 20% only when Ca-pectate or CaOx were included, and inclusion of a third component improved the NSS by greater than 20% relative to the fit value obtained with only 2 components. Thus, the Ca speciation in *cod5* vein and intervein of *cod5* and WT plants was best modeled as a mixture of Ca-citrate, Ca-pectate, and CaOx (Figure 5; Table 2). This is consistent with results presented here (Table 1) and from previous studies (Nakata and McConn, 2006), showing detectable amounts of oxalate in *cod5*. In the present study, bulk measurements indicated that 63% of the oxalate in *cod5* was found in the soluble fraction. In bulk measurements of total oxalate, WT contained  $10.5 \text{ mg g}^{-1} \text{ d.wt}$  compared to  $1 \text{ mg g}^{-1} \text{ d.wt}$  in *cod5* (Nakata and McConn, 2003). Similarly, later estimates of the molar amount of Ca sequestered as the oxalate salt were 12% for WT and 1.5% for *cod5* (Nakata and McConn, 2006).

While the WT and *cod5* plants have similar bulk leaflet Ca, *cod5* plants have approximately 25% more Ca in interveinal tissue than WT plants. One could normalize the XANES fit results based on relative Ca abundance in interveinal tissue and find that *cod5* plants have approximately 1.5 times more Ca-pectate in interveinal tissue than WT plants, and approximately 1.2 times more Ca-citrate in interveinal tissue than WT plants. Although *cod5* and WT plants have similar total Ca abundance, *cod5* lacks the insoluble  $\text{CaOx}_{(c)}$  form.

## DISCUSSION

In this study SXRF and  $\mu$ XANES have been used as tools in the functional characterization of a gene, uncovering a contrast in the Ca distribution and speciation in leaflets of *cod5*, a mutant of the model plant *Medicago trunculata* Gaertn. SXRF is increasingly used as an elemental imaging technique in plant molecular genetics because it combines potentially non-destructive spatially resolved analysis of fresh plant tissues (e.g. (Scheckel et al., 2007)) with simultaneous multi-elemental detection, and is a freely available technique.

We have shown that Ca is distributed primarily along the secondary vasculature in WT *Medicago* terminal and lateral leaflets, and that the *cod5* mutant lacks this discrete Ca distribution. We hypothesize that discrete Ca-enriched cells may be crystal idioblasts, although higher resolution light and X-ray fluorescence microscopy is required to confirm this. We have also shown key differences in the speciation of Ca between WT and *cod5* plants, with 1.5 times more Ca-pectate and 1.2 times more Ca-citrate in the interveinal tissue of *cod5* plants than WT. It is intuitive to hypothesize that in the absence of oxalate, Ca binds to these ligands, and cannot therefore participate in the  $\text{CaOx}_{(C)}$  formation in the specialized cells along the secondary vasculature.

The findings in this study lead to the hypothesis that the contrasting localization and speciation of Ca observed in *cod5* are a factor in the increased Ca bioavailability demonstrated in feeding studies using *cod5* (Morris et al., 2007). Further work remains to be done to clarify whether the Ca-rich cells are specialized crystal idioblast cells, and whether these cells still form in *cod5* leaflets.

## EXPERIMENTAL PROCEDURES

### Plant growth conditions

*Medicago truncatula* cv. Jemalong ecotype A17 seeds were nicked with a razor blade and allowed to germinate on 0.7% (w/v) agar plates. The germinated plants then were grown hydroponically as previously described (Nakata and McConn, 2006). Leaflets were harvested from 5-week old plants and freeze dried.

### Determination of bulk Ca concentration

Calcium measurements were conducted using inductively coupled plasma atomic emission absorption spectrometry on weighed leaflet samples (Soil, Water and Forage Testing Laboratory, Texas A&M University). Each measurement was done in duplicate on three independently grown sets of plants. The results were averaged and standard error calculated.

### Determination of bulk oxalate concentration

Oxalate measurements were conducted as previously described (Nakata and McConn, 2000). In brief, weighed freeze-dried leaflet samples were interveinal in water and centrifuged. The supernatant was decanted and the soluble oxalate measured using an oxalate diagnostic kit (Trinity Biotech). The amount of total oxalate was determined by omitting the centrifugation step and solubilizing the  $\text{CaOx}_{(C)}$  through the addition of  $\text{H}^+$ -Dowex in dilute acid. The mixture was heated at 60°C for 1h and the pH of the mixture adjusted (pH between 5 and 7). The mixture then was charcoal filtered and centrifuged. The supernatant was analyzed for oxalate content using an oxalate diagnostic kit (Trinity Biotech). Measurements were done in triplicate on three independently grown sets of plants, the results averaged, and standard error determined.

### Synchrotron X-ray Fluorescence mapping

Dried, intact lateral and terminal leaflets and cryo-sectioned leaflets from WT and *cod5* were imaged at beamline X27A of the National Synchrotron Light Source, a hard X-ray microprobe, with operating energies between 3.8 and 32 keV. Leaflet analysis was performed on whole, freeze-dried dehydrated (1 week) *Medicago* terminal and lateral leaflets from WT and *cod5*, to show the Ca distribution characteristics on the scale of the whole leaflet, and on 20  $\mu\text{m}$ -thick cryo-sections of fresh *Medicago* WT and *cod5* leaflets. The beam dimensions at X27A are 7×14  $\mu\text{m}$  (V×H) and flux is  $5\times 10^9$  photons/second at 10 keV. For the whole-leaflet specimens, a pixel size of 25  $\mu\text{m}$  and a dwell time of 50

milliseconds were used. To confirm the observed Ca distribution phenotype, two additional images of WT and *cod5* leaflets halved down the primary vein were collected (see supplementary information, Figure S1). These images also showed that in *cod5* the interveinal Ca distribution had higher abundances at the terminal part of the leaflet, as compared to the basal. Images of leaflet cross-sections were collected to provide a different view perspective of the Ca-enriched cells flanking the secondary veins, and to allow collection of XANES spectra directly without the interfering signals resulting from the beam passing through epidermal layers and interveinal tissue of the leaf, which also contain Ca. Image quantification was standard-based, using NRLXRF software (Criss, 1977), and expressed as  $\mu\text{g cm}^{-2}$ .

### Cryo-section preparation

Leaflets were oriented with the tip pointing upwards and placed into a well of OCT (optimal cutting temperature) embedding medium (Tissue-Tek, Torrance, CA) then rapidly cooled to  $-20^{\circ}\text{C}$  for preparation of tissue cryosections. Leaf tissue was cryotomed at  $-15^{\circ}\text{C}$  to 20  $\mu\text{m}$  thickness using a CM 1900 cryotome (Leica Microsystems, GmgH, Nussloch, Germany). Tissue sections were mounted onto ultralene film (SPEX, Metuchen, NJ) and immediately analyzed by X-ray microprobe.

### X-ray Powder Diffraction

For microbeam X-ray diffraction measurements, the monochromator was calibrated using a zirconium foil and powder diffraction patterns were collected at 17,479 eV ( $\lambda=0.7093 \text{ \AA}$ ) for 60 or 300 s using a Bruker 1500 SMART CCD area detector. A background pattern of the backing material (ultralene film) plus 20  $\mu\text{m}$  OCT compound was collected and subtracted from patterns obtained at sample regions of interest. A pattern of CaOx monohydrate standard reference material was also collected. Data processing was performed with Fit2D software.

### X-ray Absorption Near-edge Structure ( $\mu\text{XANES}$ ) Spectroscopy

For Ca K-edge  $\mu\text{XANES}$  measurements, the monochromator was calibrated using the NIST AN100 (anorthite) glass standard. The inflection point for this reference was set to 4038.5 eV and samples were scanned from 4020 to 4170 eV using 0.25 to 5 eV energy steps and 3 to 6 seconds dwell time. Corrections for self-absorption (or over-absorption) were made for whole-leaf samples using the method described by Sarret et al., (2007). Spectra were collected from both freeze-dried, dehydrated and fresh, cryosectioned samples. Data obtained from 20  $\mu\text{m}$  thick leaf cryosections were free of self-absorption effects, with the exception of the Ca-rich cells, and were used in the evaluation and correction of self-absorption for whole-leaf spectra and spectra obtained from Ca-rich cells exposed in cross-section. XANES spectra were processed using the Athena software package (Ravel and Newville, 2005). Spectra were averaged prior to edge-step normalization, and consistent data treatment was used for standards and experimental data. Linear least-squares fit analysis (LLSF) were conducted to reveal the composition of individual experimental spectra using linear combination fitting utilities from beamline 10.3.2 (<http://xraysweb.lbl.gov/uxas/Index.htm>). The goodness-of-fit was evaluated by calculating a normalized sum-squares (NSS) residual of the fit involving the inclusion of the *i*th component ( $\text{NSS} = \frac{(y - y_{\text{fit}})^2}{(y^2)}$ ). The inclusion of more than one fit component required an improvement of the linear fit by at least 20 percent and the component added must represent at least 10% of the measured signal (Sarret et al., 2007; Grafe et al., 2008). Reference materials included Ca-citrate, Ca-pectate, Ca-oxalate, Ca-nitrate, Ca-sulfate, Ca-chloride, Ca-phosphate (apatite), and Ca-carbonate (calcite).

## Supplementary Material

Refer to Web version on PubMed Central for supplementary material.

## Acknowledgments

The authors would like to thank Megan Bourassa for her work on the cryosectioning of Medicago leaf samples. This work was supported by grants from the National Institute of Environmental Health Sciences, (Superfund Research Program P42 ES007373-17), the Children's Environmental Health and Disease Prevention Center (P20 ES018175 and RD-83459901) to TP, and to KH by the U.S. Department of Agriculture/Agricultural Research Service (under cooperative agreement 58-62650-6001), and the U.S. Department of Agriculture Grant CSRESS#2005-34402-16401 Designing Foods for Health and to PAN by the U.S. Department of Agriculture/Agricultural Research Service (under cooperative agreement 58-6250-0-008) Portions of this work were performed at Beamline X27A, National Synchrotron Light Source (NSLS), Brookhaven National Laboratory. X27A is supported in part by the U.S. Department of Energy - Geosciences (DE-FG02-92ER14244 to The University of Chicago - CARS) and Brookhaven National Laboratory– Department of Environmental Sciences. Use of the NSLS was supported by the DOE under Contract No. DEAC02-98CH10886.

## REFERENCES

- Bauer P, Elbaum R, Weiss IM. Calcium and silicon mineralization in land plants: Transport, structure and function. *Plant Science*. 2011; 180:746–756. [PubMed: 21497710]
- Criss, JW. NRLXRF, A FORTRAN program for X-ray fluorescence analysis. Washington, D.C.: Naval Research Laboratory; 1977.
- Franceschi VR, Horner HT. Calcium oxalate crystals in plants. *Botanical Reviews*. 1980; 46:184–193.
- Franceschi VR, Nakata PA. Calcium oxalate in plants: Formation and function. *Annual Review of Plant Biology*. 2005; 56:41–71.
- Grafe M, Tappero RV, Marcus MA, Sparks DL. Arsenic speciation in multiple metal environments: I. Bulk-XAFS spectroscopy of model and mixed compounds. *Journal of colloid and interface science*. 2008; 320:383–399. [PubMed: 18262202]
- Horner HT, Zindler-Frank E. Histochemical, spectroscopic, and X-ray diffraction identifications of the two forms of calcium oxalate in three legumes and *Begonia* Canadian. *Journal of Botany*. 1982; 60:1021–1027.
- Kim SA, Punshon T, Lanzirotti A, Liangtao L, Alonso JM, Ecker JR, Kaplan J, Guerinot ML. Localization of iron in *Arabidopsis* seed requires the vacuolar membrane transporter VIT1. *Science*. 2006; 314:1295–1298. [PubMed: 17082420]
- Korth KL, Dege SJ, Park S-H, Goggin FL, Wang Q, Gomez SK, Liu G, Jia L, Nakata PA. Medicago trunculata mutants demonstrate the role of plant calcium oxalate crystals as an effective defense against chewing insects. *Plant Physiol*. 2006; 141:188–195. [PubMed: 16514014]
- McNair JB. The interrelations between substances in plants: essential oils and resins, cyanogen and oxalate. *American Journal of Botany*. 1932; 19:255–271.
- Morris J, Nakata PA, McConn M, Brock A, Hirschi KD. Increased calcium bioavailability in mice fed genetically engineered plants lacking calcium oxalate. *Plant Mol Biol*. 2007; 64:613–618. [PubMed: 17514431]
- Nakata PA. Advances in our understanding of calcium oxalate crystal formation and function in plants. *Plant Science*. 2003; 164:901–909.
- Nakata PA. Engineering calcium oxalate crystal formation in *Arabidopsis*. *Plant Cell Physiology*. 2012; 53:1275–1282. [PubMed: 22576773]
- Nakata PA, McConn MM. Isolation of Medicago trunculata mutants defective in calcium oxalate crystal formation. *Plant Physiol*. 2000; 124:1097–1104. [PubMed: 11080287]
- Nakata PA, McConn MM. Calcium oxalate crystal formation is not essential for growth of Medicago trunculata. *Plant Physiology and Biochemistry*. 2003; 41:325–329.
- Nakata PA, McConn MM. A genetic mutation that reduces calcium oxalate content increases calcium availability in Medicago trunculata. *Functional Plant Biology*. 2006; 33:703–706.
- Punshon T, Ricachenevsky FK, Hindt MF, Socha A, Zuber H. Methodological approaches for using synchrotron X-ray fluorescence (SXRF) imaging as a tool in ionic characterization: Examples

from whole plant imaging of *Arabidopsis thaliana*. *Metallomics*. 2013; 5:1133–1145. [PubMed: 23912758]

Ravel B, Newville M. ATHENA, ARTEMIS, HEHAESTUS: data analysis for X-ray absorption spectroscopy using IFEFFIT. *Journal of Synchrotron Radiation*. 2005; 12:537–541. [PubMed: 15968136]

Sarret G, Isaure M-P, Marcus MA, Harada E, Choi Y-E, Fakra S, Manceau A. Chemical forms of calcium in Ca,Zn- and Ca,Cd- containing grains excreted by tobacco trichomes. *Canadian Journal of Chemistry*. 2007; 85:738–746.

Schadel WE, Walter Jr WM. Calcium oxalate crystals in the roots of sweet potato. *Journal of the American Society of Horticultural Science*. 1980; 105:851–854.

Scheckel KG, Hamon RE, Jassogne L, Rivers M, Lombi E. Synchrotron x-ray absorption computed microtomography imaging of thallium compartmentalization in *Iberis intermedia*. *Plant and Soil*. 2007; 290:51–60.

Webb MA. Cell-mediated crystallization of calcium oxalate in plants. *The Plant Cell*. 1999; 11:751–761. [PubMed: 10213791]

Yamauchi D, Tamaoki D, Hayami M, Takeuchi M, Karahara I, Sato M, Toyooka K, Nishioka H, Terada Y, Uesugi K, Takano H, Kagoshima Y, Mineyuki Y. Micro-CT observations of the 3D distribution of calcium oxalate crystals in cotyledons during maturation and germination in *Lotus miyakojimae* seeds. *Microscopy*. 2013; 62:353–361. [PubMed: 23220770]

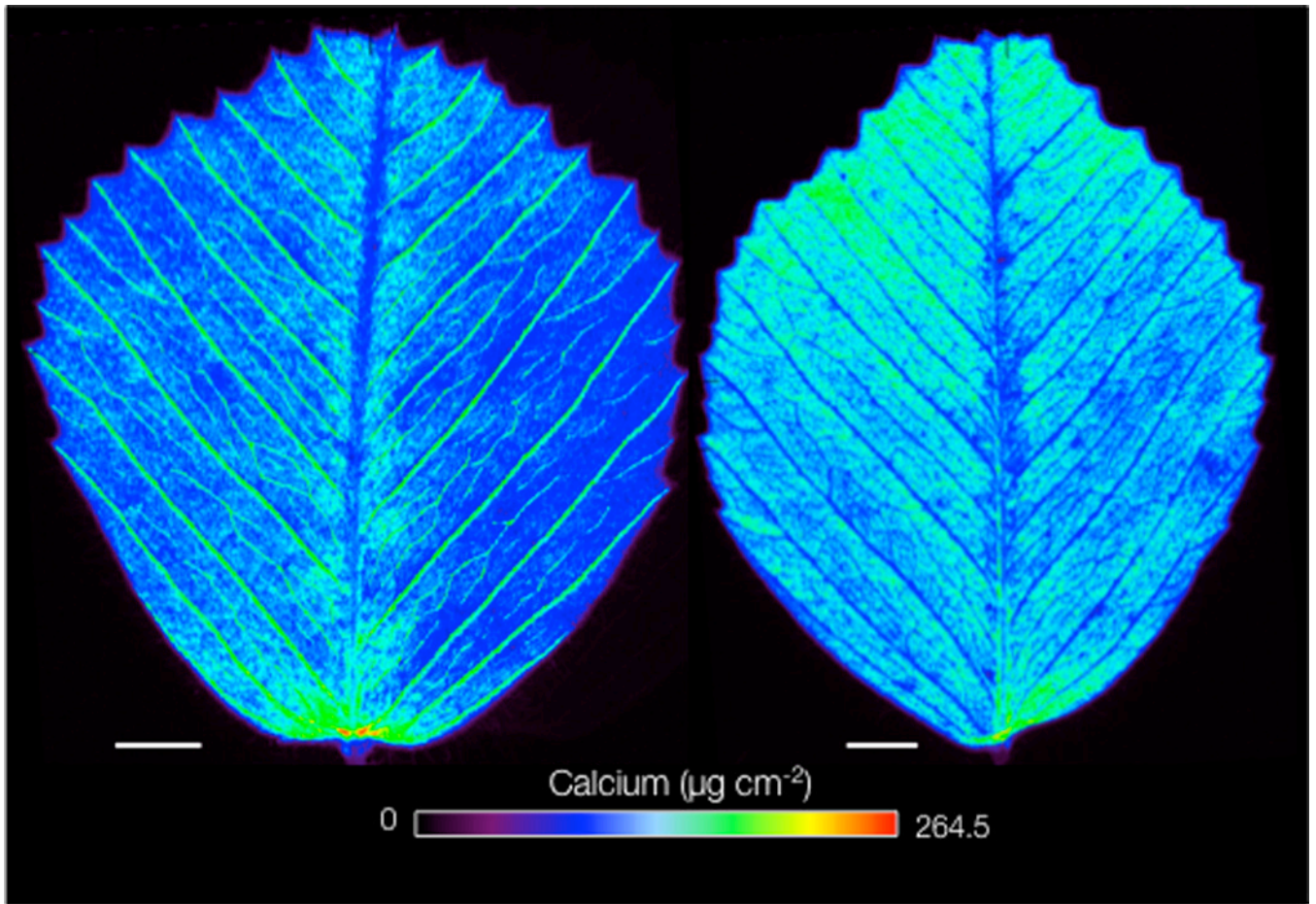


**Figure 1.** Synchrotron X-ray fluorescence image of Ca in leaves of *Medicago truncatula* wild type (WT) and calcium oxalate deficient 5 (*cod5*) mutant. Data is shown as maximum pixel abundance in  $\mu\text{g cm}^{-2}$ , scale bar is 2 mm.

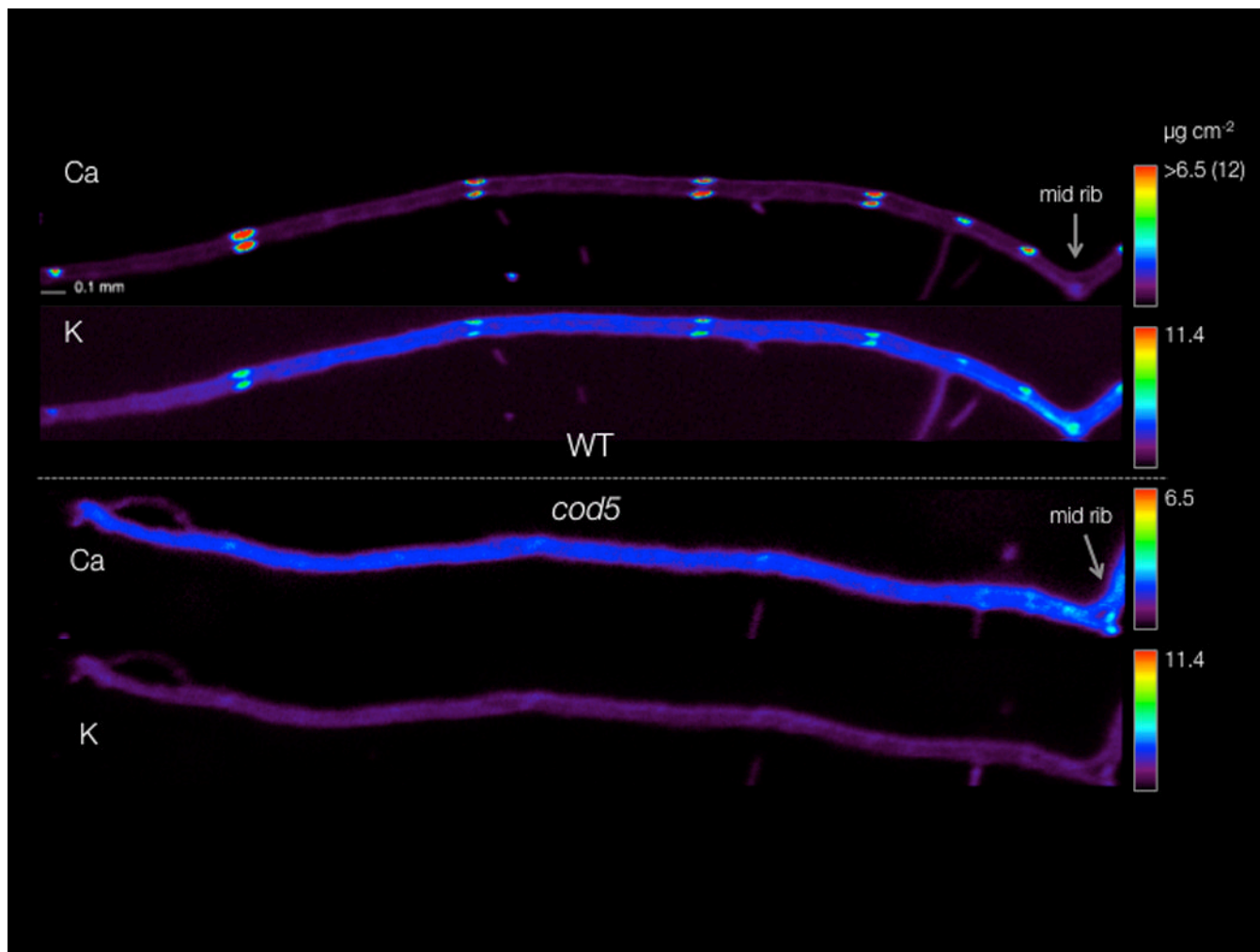


**Figure 2.** Synchrotron X-ray fluorescence image of Ca and K in cryo-sectioned fresh leaf cross sections from WT and *cod5*. The color legend shows the maximum pixel abundance in  $\mu\text{g cm}^{-2}$ . Each element has been scaled to a common value to show abundance differences. For K, the maximum of the WT image has been used. Ca images are scaled to an intermediate value to prevent information loss, and the true maximum is shown in parentheses.

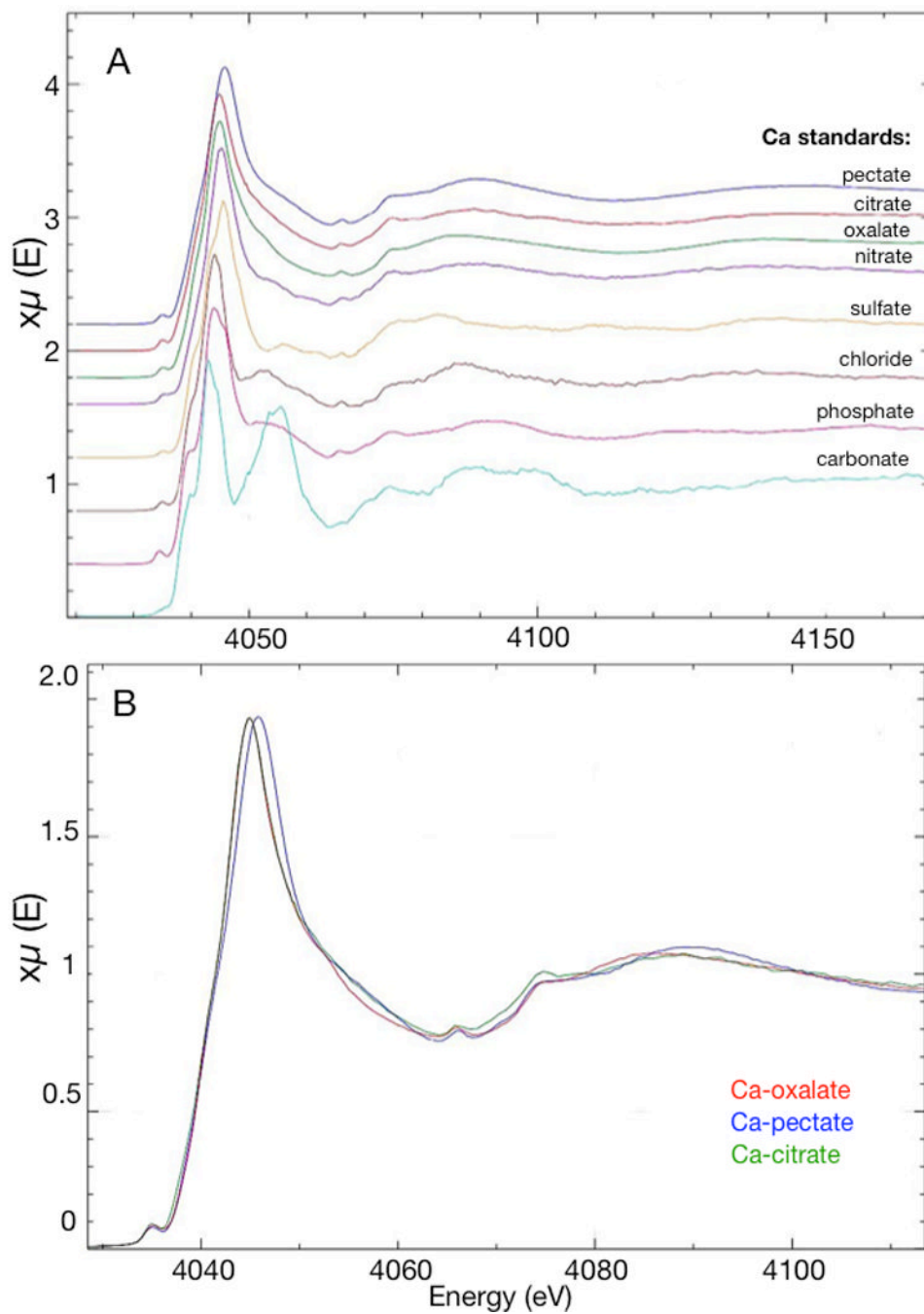


**Figure 3.** A. Ca K-edge  $\mu$ XANES spectra for the reference compounds considered in the linear combination fits and B. enlargement of the main peaks for Ca-pectate, Ca-oxalate, and Ca-citrate.

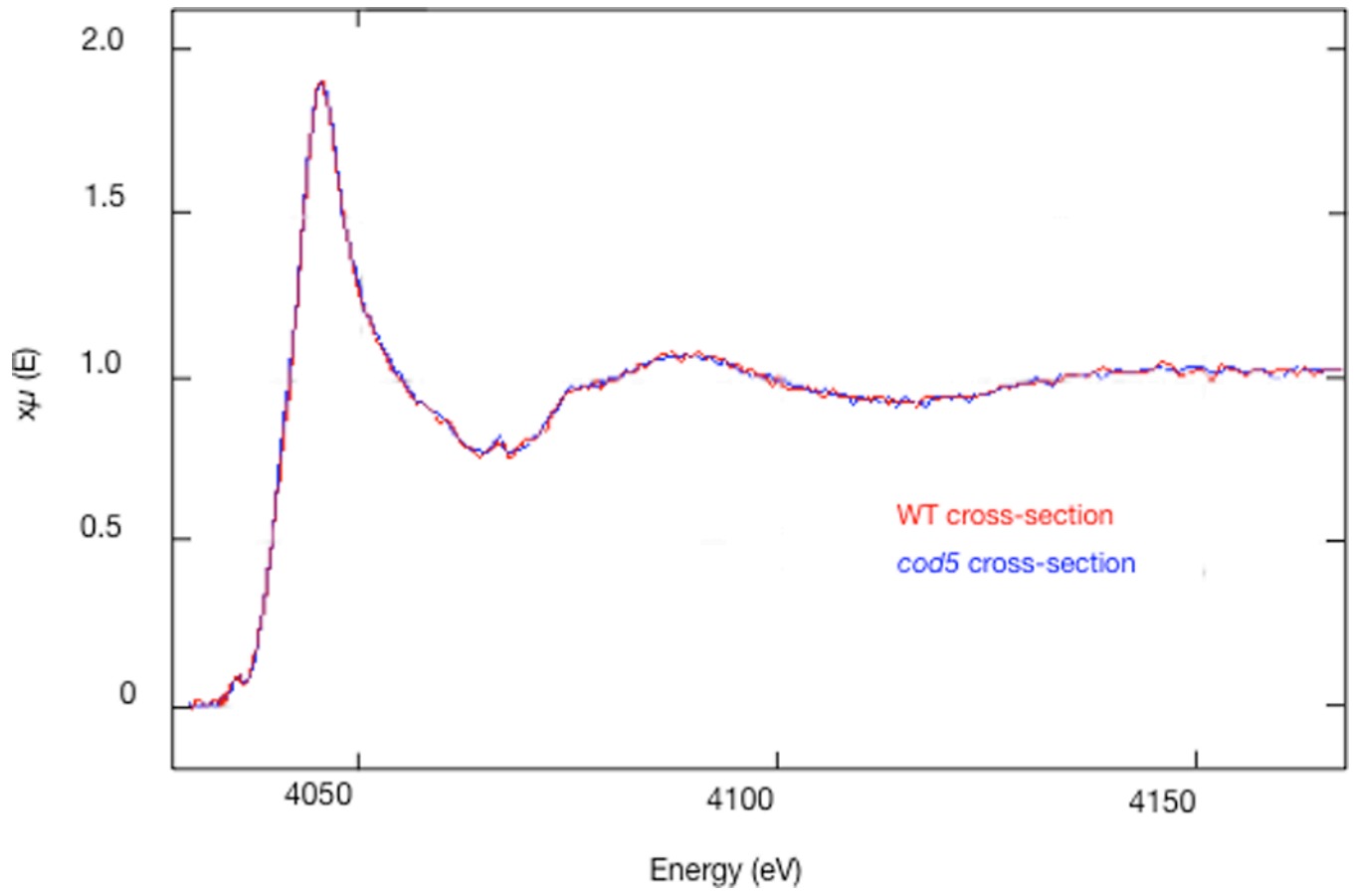


**Figure 4.** Overplot of Ca K-edge  $\mu$ XANES spectra of leaf tissue cross-sections (*cod5* XS & WT XS) showing the similarity in Ca speciation for the interveinal tissue of WT and *cod5* plants.

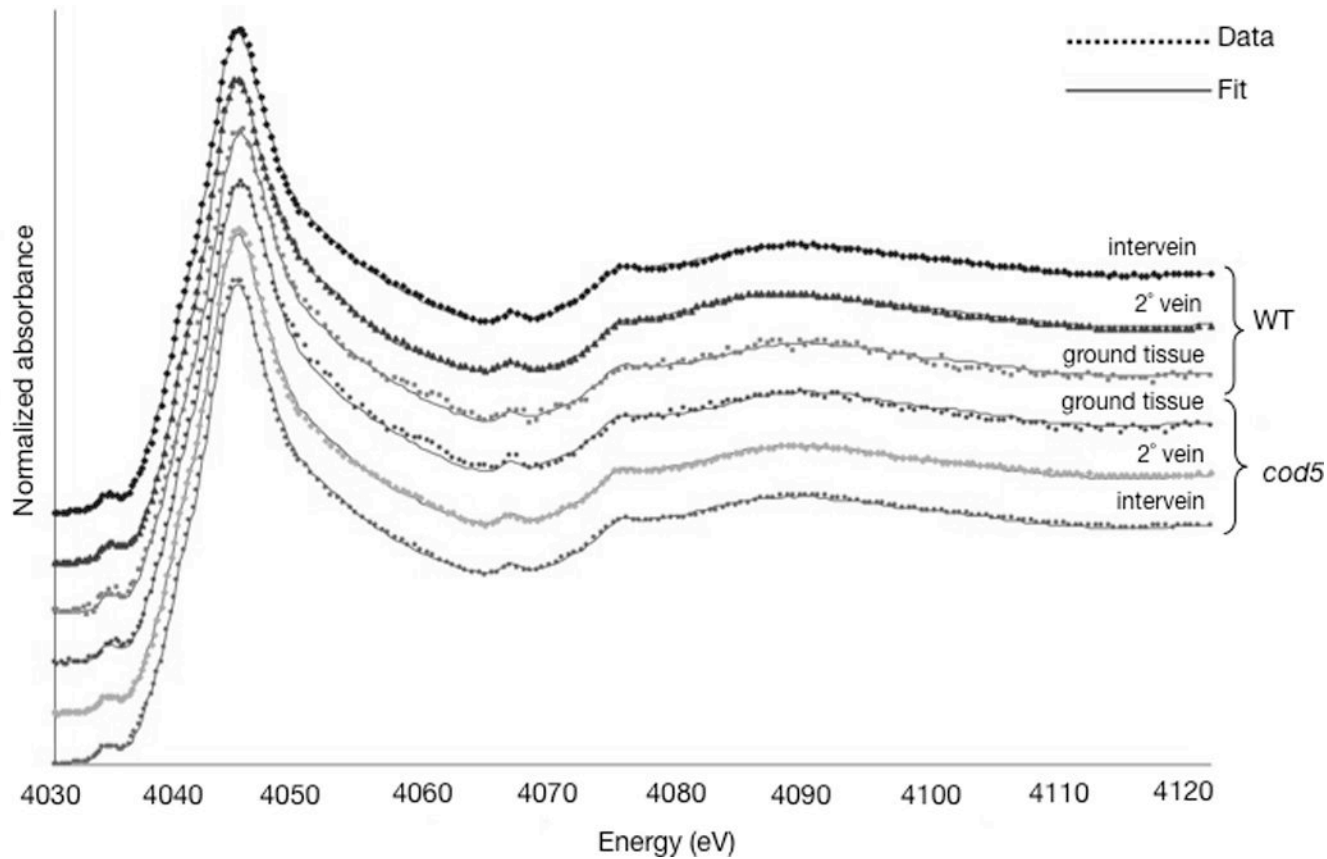


**Figure 5.** Ca K-edge  $\mu$ XANES spectra for wildtype (WT) and mutant (*cod5*) leaf and 20 $\mu$ m thick leaf tissue cross-sections and corresponding linear combination fits. All spectra except cross-sections were corrected for self-absorption.

**Table 1**

. Concentration of oxalate determined in water extracts of ground, freeze-dry WT and *cod5* leaves via colourimetric assay, and the concentrations of Ca and K determined by ICP (Expressed as mg g<sup>-1</sup> dry weight).

	Oxalate		Calcium	Potassium
	Total	Soluble		
WT	16.9 (±0.2)	1.2 (±0.1)	16.7 (± 1.8)	25.5 (±1.0)
<i>cod5</i>	1.9 (±0.1)	1.2 (±0.0)	17.7 (±1.2)	26.1 (±0.6)

Table 2

Ca XANES fit results.

Line	POI	a	CaCit	CaPec	CaOx	I	NSS	dE
			%					
<i>cod5</i>	v	13	<b>35</b>	<b>24</b>	<b>41</b>	38	9.01e-05	0.09
<i>cod5</i>	iv	17	<b>41</b>	<b>17</b>	<b>41</b>	28	7.32e-05	0.06
WT	iv	23	<b>44</b>	<b>25</b>	<b>32</b>	45	7.55e-05	0.11
WT	v	39		<b>10</b>	<b>90</b>	21	5.58e-05	0.01
<i>cod5</i> (XS)	meso	<b>0</b>	<b>58</b>	<b>43</b>		42	3.07e-04	0.04
WT (XS)	meso	<b>0</b>	<b>65</b>	<b>36</b>		36	2.67e-04	-0.02

a = Coefficient of self-absorption

I = % improvement of fit  $[100 - (\text{NSS } 2C^*100/\text{NSS } 1C)]$ 

NSS = normalized sum squares

dE = Energy shift in eV